

## Electronic properties of artificial Au chains with individual Pd impurities

T. M. Wallis,<sup>a)</sup> N. Nilius,<sup>b)</sup> G. Mikaelian, and W. Ho<sup>c)</sup>

*Department of Physics and Astronomy and Department of Chemistry, University of California, Irvine, California 92697-4675*

(Received 21 October 2004; accepted 9 November 2004; published online 14 December 2004)

Artificial Au atomic chains with individual Pd impurities were assembled from single metal atoms with a scanning tunneling microscope on a NiAl(110) surface. Scanning tunneling spectroscopy (STS) revealed an electronic resonance 2.15 eV above the Fermi energy localized within 4 Å of single Pd atom impurities and two electronic resonances 2.25 eV and 2.95 eV above the Fermi energy localized within 8 Å of Pd dimer impurities. The emergence of these localized resonances was studied by STS at each stage of the atom-by-atom assembly. Additionally, conductance images of the chains revealed delocalized electronic density oscillations in the pure Au segments of the chains. © 2005 American Institute of Physics. [DOI: 10.1063/1.1842712]

The electronic properties of nanostructures consisting of only a few atoms may depend sensitively on the exact position and chemical identity of each and every atom in the structure. For example, calculations for nanowires<sup>1,2</sup> and experiments on point contacts<sup>3</sup> indicate that the transport properties of atomic scale conductors may be altered considerably by a single atom impurity. The scanning tunneling microscope (STM) is a useful tool for investigating the electronic properties of nanostructures consisting of a small number of atoms due to its capability of probing electronic structure with high spatial resolution. STM has been used to investigate individual electronic wavefunctions of metallic single-walled carbon nanotubes,<sup>4</sup> surface states on nanoscale Ag islands on Ag(111),<sup>5</sup> and electron scattering from single defects in carbon nanotubes.<sup>6</sup> The additional capability of the STM to laterally manipulate individual atoms makes it possible to construct custom nanostructures such as quantum corrals.<sup>7,8</sup>

We recently reported a new strategy for the atom-by-atom assembly and electronic characterization of Au atomic chains on NiAl(110) by STM. Conductance ( $dI/dV$ ) images revealed electronic density oscillations delocalized along the entire length of the Au chains.<sup>9</sup> The dispersion relation and effective electron mass for the Au chains were determined by spatially resolved scanning tunneling spectroscopy (STS).<sup>10</sup> Recently, Folsch and co-workers used similar techniques to characterize artificial Cu chains on Cu(111).<sup>11</sup> Here, we extend this strategy to Au atomic chains with single Pd atom and Pd dimer impurities on NiAl(110). The energy and spatial extent of individual, localized impurity resonances is directly measured by STS. Additionally, the evolution of the localized resonances is monitored at each stage of the atom-by-atom assembly of the chains. Finally,  $dI/dV$  imaging re-

veals delocalized electronic density oscillations in the pure Au segments of the chains.

The homemade STM used in these experiments has been detailed elsewhere.<sup>12</sup> The STM was operated at 11 K and in ultrahigh vacuum (base pressure  $\sim 3 \times 10^{-11}$  torr). A small number ( $\sim 0.001$  monolayer) of individual Au and Pd atoms were evaporated *in situ* onto the clean NiAl(110) surface at 11 K from two separately heated alumina crucibles. During STS measurements and  $dI/dV$  imaging, the differential tunneling conductance was obtained using a lockin technique. Automated software controlled the acquisition of  $dI/dV$  spectra at fixed intervals along the chain. Periodic lateral tracking of a local maximum in apparent height was used during STS measurements to compensate for thermal drift. The STM feedback loop was off during  $dI/dV$  measurements, but was on during all tip movement and tracking procedures.  $dI/dV$  images were acquired using a technique previously described for  $dI/dV$  imaging of pure Au chains.<sup>9</sup>

Individual Au and Pd atoms appear as round protrusions in constant-current topographic images. STS measurements with the tip positioned above single Au atoms adsorbed on Ni-Ni bridge sites reveal an electronic resonance 2.00 eV above the Fermi energy which is not observed with the tip positioned over the bare NiAl surface. STS measurements with the tip positioned above single Pd atoms on Ni-Ni bridge sites reveal an electronic resonance at 2.90 eV. These electronic resonances are attributed to the hybridization of the Au  $6sp$  and Pd  $5sp$  orbitals with the NiAl electronic states. These differences in the electronic structure of Au and Pd atoms are reflected in a strong voltage dependence of the apparent heights of these atoms in topographic images. In topographic images taken with a sample bias voltage near 2.00 V, Au atoms have a large apparent height and are easily distinguished from Pd atoms.

Linear atomic chains were assembled along the [001] direction of NiAl(110) via repeated manipulations of individual Au and Pd atoms with the STM tip. The capability of the STM to position individual atoms and the quasi-one-dimensional template provided by the NiAl substrate make it possible to assemble nanostructures with a precise knowl-

<sup>a)</sup>Present Address: National Institute of Standards and Technology, Boulder, CO 80305.

<sup>b)</sup>Present Address: Fritz-Haber-Institut, Faradayweg 4-6, D-14195 Berlin, Germany.

<sup>c)</sup>Author to whom correspondence should be addressed. Electronic mail: wilsonho@uci.edu

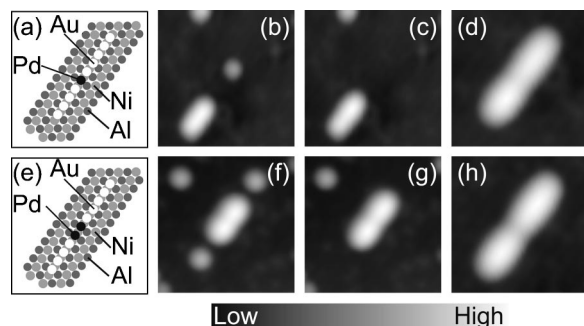


FIG. 1. Construction of Au chains with Pd impurities: (a) Schematic diagram of a  $\text{Au}_5\text{PdAu}_4$  chain on  $\text{NiAl}(110)$ . (b)–(c) Consecutive topographic images show a single Au atom added to a  $\text{Au}_2\text{PdAu}_2$  chain to make a  $\text{Au}_3\text{PdAu}_2$  chain (sample bias voltage  $V_{\text{sample}} = 1.00$  V, tunneling current  $I_{\text{tunnel}} = 1.00$  nA). Both images are  $63 \text{ \AA} \times 63 \text{ \AA}$ . (d) A topographic image of  $\text{Au}_5\text{PdAu}_4$  chain ( $V_{\text{sample}} = 1.00$  V,  $I_{\text{tunnel}} = 1.00$  nA). Image size is  $44 \text{ \AA} \times 44 \text{ \AA}$ . (e) Schematic diagram of a  $\text{Au}_5\text{Pd}_2\text{Au}_4$  chain on  $\text{NiAl}(110)$ . (f)–(g) Consecutive topographic images show two Au atoms added to a  $\text{Au}_2\text{Pd}_2\text{Au}_2$  chain to make a  $\text{Au}_3\text{Pd}_2\text{Au}_3$  chain ( $V_{\text{sample}} = 1.52$  V,  $I_{\text{tunnel}} = 1.00$  nA). Both images are  $63 \text{ \AA} \times 63 \text{ \AA}$ . (h) A topographic image of  $\text{Au}_5\text{Pd}_2\text{Au}_4$  chain ( $V_{\text{sample}} = 1.00$  V,  $I_{\text{tunnel}} = 1.00$  nA). Image size is  $44 \text{ \AA} \times 44 \text{ \AA}$ . The palette used in the topographic images corresponds to a range of about  $3 \text{ \AA}$ .

edge of the arrangement of each and every atom within the structures. Two different structures were assembled: a single Pd atom impurity embedded between five- and four-atom Au segments ( $\text{Au}_5\text{PdAu}_4$ ) as well as a Pd dimer impurity embedded between five- and four-atom Au segments ( $\text{Au}_5\text{Pd}_2\text{Au}_4$ ), as illustrated in Figs. 1(a) and 1(e), respectively. All atoms within the chains were positioned on Ni-Ni bridge sites. During assembly, individual Au atoms were sequentially added to the ends of the chains, as shown in Figs. 1(b)–1(c), 1(f)–1(g). In topographic images such as Figs. 1(d) and 1(h), the Pd impurities appear slightly narrower than the rest of the otherwise uniform chain.

The electronic properties of each structure were studied by performing STS at a series of tip positions along the length of each chain, as shown in Fig. 2. STS measurements taken with the tip positioned above the single atom and diatomic impurities display peaks in  $dI/dV$  at 2.15 eV and 2.25 eV, respectively. These impurity resonances are localized within  $4 \text{ \AA}$  of the single Pd impurity and  $8 \text{ \AA}$  of the Pd dimer impurity. Near the Pd dimer impurity in the  $\text{Au}_5\text{Pd}_2\text{Au}_4$  chain, a second feature between 2.70 eV and 3.00 eV is observed as a shoulder, but its exact energy is difficult to assign due to the sharply rising background signal in that energy range for this chain. Based on STS measurements on a different  $\text{Au}_5\text{Pd}_2\text{Au}_4$  chain, shown in Fig. 3(b) and discussed below, this feature's energy is assigned as 2.95 eV. The single Pd impurity resonance is shifted down 0.75 eV from the 2.90 eV resonance observed for isolated Pd atoms [dashed line in Fig. 2(a)], reflecting interactions with the nearby Au atoms. The dimer impurity states are shifted up 0.15 eV and 0.30 eV relative to the resonances of an isolated Pd dimer at 2.10 eV and 2.65 eV [dashed line in Fig. 2(b)]. These smaller shifts reflect the strength of the Pd–Pd bond and weaker interactions with the nearby Au atoms.

The emergence of these localized impurity resonances were studied by measuring the  $dI/dV$  spectra of the chains at

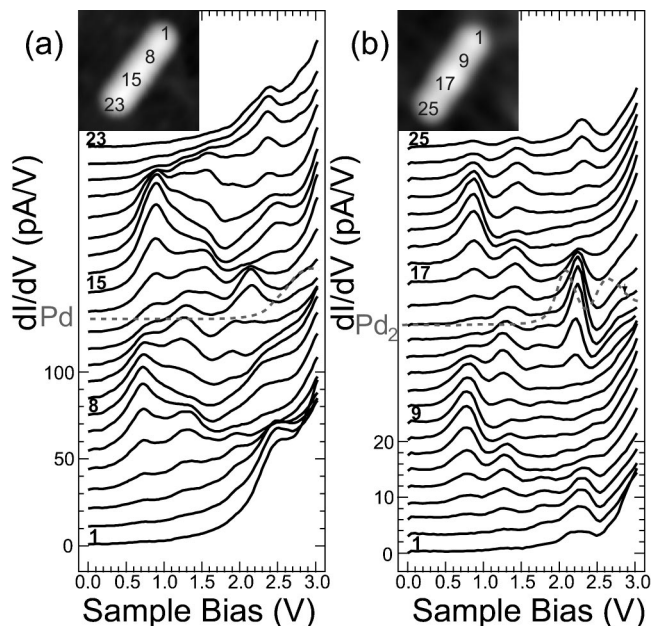


FIG. 2. (a) 23 spectra obtained by scanning tunneling spectroscopy (STS), acquired at fixed intervals along the length of the  $\text{Au}_5\text{PdAu}_4$  chain. In the inset, an image is labeled to indicate the positions at which the spectra were acquired. For each spectrum, tip-sample distance was fixed with  $V_{\text{sample}} = 2.98$  V and  $I_{\text{tunnel}} = 1.00$  nA. The STS spectrum of an isolated Pd atom (dashed line) is shown for comparison. (b) 25 STS spectra acquired at fixed intervals along the length of the  $\text{Au}_5\text{Pd}_2\text{Au}_4$  chain. Spectral positions are shown in the inset. For each spectrum, tip-sample distance was fixed with  $V_{\text{sample}} = 3.06$  V and  $I_{\text{tunnel}} = 0.10$  nA. The STS spectrum of an isolated Pd dimer (dashed line) is shown for comparison. The isolated Pd atom and Pd dimer spectra in (a) and (b), respectively, have been scaled to facilitate comparison.

various stages of assembly. STS measurements were taken with the tip positioned above the Pd impurities as each chain was constructed atom-by-atom ( $\text{Pd}, \text{AuPd}, \text{AuPdAu}, \text{Au}_2\text{PdAu}, \dots, \text{Au}_m\text{PdAu}_n$ ), as shown in Fig. 3. The  $dI/dV$  spectrum of an AuPd dimer displays two peaks at 1.70 eV and 2.75 eV which are shifted down from the peaks of isolated Au and Pd monomers at 2.00 eV and 2.90 eV, respectively. The further addition of Au atoms to form a AuPdAu trimer and a  $\text{Au}_2\text{PdAu}$  tetramer results in additional peaks in the  $dI/dV$  spectra and downward shifts of the lowest energy peak. This behavior resembles the evolution of short, pure Au chains. When two atoms have been added to each side of the Pd atom impurity ( $m = 2, n = 2$ ), the localized electronic resonance at 2.15 eV abruptly emerges. Further addition of Au atoms has no effect on the energy of this localized resonance, but the lowest energy peak continues to shift down in energy. In the  $\text{Au}_m\text{Pd}_2\text{Au}_n$  series of chains, localized impurity resonances at 2.25 eV and 2.95 eV also emerge abruptly, but at  $m = 2, n = 1$ . Once again, the further addition of the Au atoms to the chain has no effect on the energy of these localized resonances.

In addition to the resonances localized on the Pd impurities, the STS measurements shown in Fig. 2 also reveal electronic features within the Au segments of the chains. The spatial distribution of the  $dI/dV$  patterns of the  $\text{Au}_5\text{PdAu}_4$  chain was studied by  $dI/dV$  imaging. Three  $dI/dV$  images of the  $\text{Au}_5\text{PdAu}_4$  chain are shown in Figs. 4(a)–4(c).

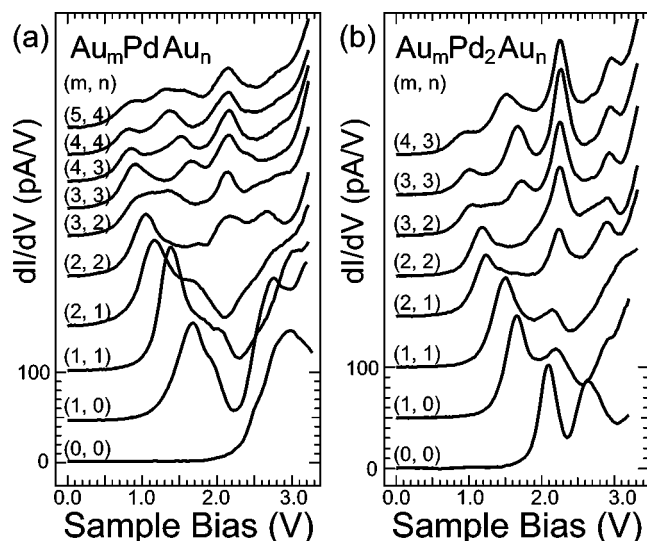


FIG. 3. Evolution of localized resonances at impurities. (a) STS of an Au chain with a single Pd impurity acquired at each step of construction from isolated Pd atom to  $\text{Au}_5\text{PdAu}_4$ . Each spectrum was acquired with the tip directly above the Pd atom. (b) STS of a Au chain with a Pd dimer impurity acquired at each step of construction from isolated  $\text{Pd}_2$  dimer to  $\text{Au}_4\text{Pd}_2\text{Au}_3$ . Each spectrum was acquired with the tip directly above the center of the  $\text{Pd}_2$  dimer. The tip sample distance was set with  $V_{\text{sample}}$  between 2.85 and 3.00 V and  $I_{\text{tunnel}} = 1.00$  nA.

Energy-dependent electronic density oscillation patterns are evident. There is one node in the five-atom Au segment and zero nodes in the four-atom Au segment in the 1.00 V  $dI/dV$  image and one node in the each Au segment in the 1.30 V  $dI/dV$  image. In Fig. 4(d), cross sections of  $dI/dV$  images reveal the evolution of the electronic density patterns in the  $\text{Au}_5\text{PdAu}_4$  chain as a function of energy.

Comparisons between the electronic density oscillations in the chains with Pd impurities and pure Au chains demonstrate that the five- and four-atom Au segments are weakly coupled to one another. In a pure 20-atom Au chain, the lowest-energy  $dI/dV$  peak was at 0.75 eV and present in STS spectra taken at all points within the interior of the chain.<sup>10</sup> Here, the lowest energy feature is 0.74 eV (0.75 eV) in the five-atom Au segment of the  $\text{Au}_5\text{PdAu}_4$  ( $\text{Au}_5\text{Pd}_2\text{Au}_4$ ) chain but shifts to 0.88 eV (0.89 eV) in the four-atom Au segment. These lowest-lying energy resonances are delocalized within either Au segment, but not along the entire chain. The 0.14 eV shift between the lowest energy peaks in the five- and four-atom Au segments is comparable to the 0.15 eV shift between the lowest energy peaks in isolated, pure, five- and four-atom Au chains. Additionally, the number and energies of peaks in the Au segments of the chains with impurities closely resembles their isolated, pure Au counterparts.

Previously, the electronic density oscillations in pure Au chains were modeled as states in a one-dimensional box potential in which the ends of the chain were the walls of the box.<sup>9,10</sup> Based on the similarity between the Au segments in  $\text{Au}_5\text{PdAu}_4$  and  $\text{Au}_5\text{Pd}_2\text{Au}_4$  with pure five- and four-atom Au chains, the Au segments of Au chains with Pd impurities may be crudely modeled as two independent particle-in-a-box systems, with each box bounded by one end of the chain and

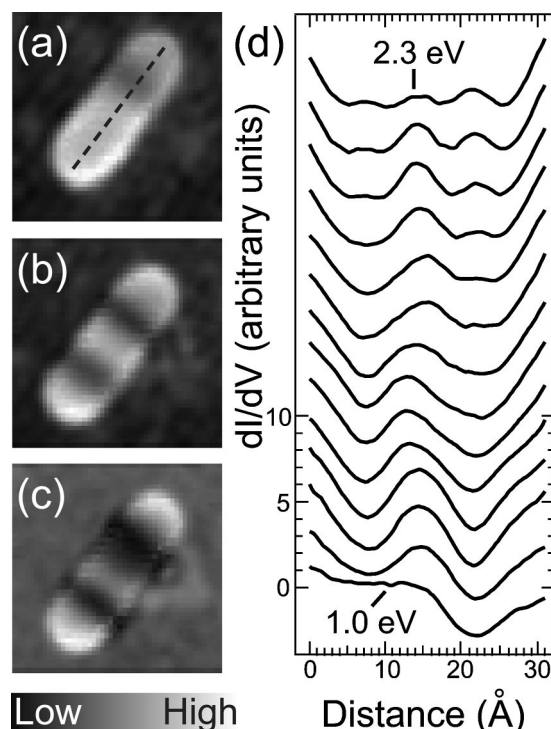


FIG. 4.  $dI/dV$  images of the  $\text{Au}_5\text{PdAu}_4$  chain taken at (a) 1.00 V, (b) 1.30 V, and (c) 1.60 V. Each curve in (d) is a cross section of a  $dI/dV$  image of the  $\text{Au}_5\text{PdAu}_4$  chain. The dashed line in (a) illustrates the location of the cross sections. The cross sections are displayed in order of increasing  $V_{\text{sample}}$  from bottom (1.00 V) to top (2.30 V) in 0.10 V increments. The curves have been offset to facilitate comparison. The cross sections are displayed such that the four-atom Au segment is on the left hand side.

the impurity. In this model, electronic density oscillations with zero, one, or two nodes correspond to the ground, first-excited, and second-excited states of the particle-in-a-box. The wavelengths of the second-excited states in the five-atom segments of both  $\text{Au}_5\text{PdAu}_4$  and  $\text{Au}_5\text{Pd}_2\text{Au}_4$  were taken from the cross sections of  $dI/dV$  images and correspond to a box  $18.0 \pm 1.0$  Å long, in agreement with the apparent size of an isolated five-atom chain in STM images. A rigorous electronic structure calculation with molecular orbital and density functional theories provides a rationalization for the application of the particle-in-a-box model to artificial Au chains on NiAl(110).<sup>13</sup>

Linear Au atomic chains with different types of Pd impurities were assembled from single metal atoms. The predominant electronic features—localized impurity resonances and delocalized density oscillations within the Au segments—were characterized by STS and  $dI/dV$  imaging. These experiments demonstrate a strategy for assembly and characterization of nanostructures with sensitivity to the position and chemical identity of each and every atom in the structure.

This work was supported by the National Science Foundation under Grant No. 0102887. N.N. gratefully acknowledges the Deutsche Forschungsgemeinschaft for support.

<sup>1</sup>H. Mehrez, A. Wlasenko, B. Larade, J. Taylor, P. Grutter, and H. Guo, Phys. Rev. B **65**, 195419 (2002).

- <sup>2</sup>N. Papanikolaou, J. Opitz, P. Zahn, and I. Mertig, *Phys. Rev. B* **66**, 165441 (2002).
- <sup>3</sup>A. Enomoto, S. Kurokawa, and A. Sakai, *Phys. Rev. B* **65**, 125410 (2002).
- <sup>4</sup>S. G. Lemay, J. W. Janssen, M. van den Hout, M. Mooij, M. J. Bronikowski, P. A. Willis, R. E. Smalley, L. P. Kouwenhoven, and C. Dekker, *Nature (London)* **412**, 617 (2001).
- <sup>5</sup>J. T. Li, W. D. Schneider, R. Berndt, and S. Crampin, *Phys. Rev. Lett.* **80**, 3332 (1998).
- <sup>6</sup>M. Ouyang, J.-L. Huang, and C. M. Lieber, *Phys. Rev. Lett.* **88**, 066804 (2002).
- <sup>7</sup>M. F. Crommie, C. P. Lutz, and D. M. Eigler, *Science* **262**, 218 (1993).
- <sup>8</sup>E. J. Heller, M. F. Crommie, C. P. Lutz, and D. M. Eigler, *Nature (London)* **369**, 464 (1994).
- <sup>9</sup>T. M. Wallis, N. Nilius, and W. Ho, *Phys. Rev. Lett.* **89**, 236802 (2002).
- <sup>10</sup>N. Nilius, T. M. Wallis, and W. Ho, *Science* **297**, 1853 (2002).
- <sup>11</sup>S. Folsch, P. Hyldgaard, R. Koch, and K. H. Ploog, *Phys. Rev. Lett.* **92**, 056803 (2004).
- <sup>12</sup>B. C. Stipe, M. A. Rezaei, and W. Ho, *Rev. Sci. Instrum.* **70**, 137 (1999).
- <sup>13</sup>G. Mills, B. Wang, W. Ho, and H. Metiu, *J. Chem. Phys.* **120**, 7738 (2004).